Stabilizing $LiCoO_2$ at 4.6 V by regulating the anti-oxidative solvents

Hengyu Ren[1,#], Guorui Zheng[1,2,#,], Yuhang Li[2], Shiming Chen[1], Xiaohu Wang[1], Mingzheng Zhang[1], Wenguang Zhao[1], Haocong Yi[1], Weiyuan Huang[3], Jianjun Fang[1,4], Tongchao Liu[3], Luyi Yang[1], Ming Liu[2,*], Qinghe Zhao[1,*], and Feng Pan[1,*]*

[1]School of Advanced Materials, Peking University Shenzhen Graduate School, Peking University, Shenzhen 518055, P. R. China.

[2]Institute of Materials Research, Tsinghua Shenzhen International Graduate School, Tsinghua University, Shenzhen 518055, P. R. China.

[3]Chemical Sciences and Engineering Division, Argonne National Laboratory, Lemont, IL 60439, USA.

[4]Qiantu battery Technology Co., Ltd, Dongguan 523808, P. R. China.

[#]These authors contributed equally.

[*]Corresponding authors. E-mail: zhengguorui1991@163.com (G. Z.); liuming@sz.tsinghua.edu.cn (M. L.); zhaoqh@pku.edu.cn (Q. Z.); panfeng@pkusz.edu.cn (F. P.).

Keywords: high-voltage $LiCoO_2$, cathode/electrolyte interphase, corrosive species, solvation structure, Co/O loss

Abstract

For $LiCoO_2$ (LCO) operated at high voltages (>4.5 V vs. Li/Li^+), the intensive side reactions between LCO and traditional ethylene carbonate (EC) based electrolytes with $LiPF_6$ salt can produce plenty of corrosive species (such as HF, HPO_2F_2, etc.), causing severe surface degradation. Herein, the anti-oxidative fluoroethylene carbonate (FEC) and difluoroethylene carbonate (DFEC) are selected as co-solvents to reduce the generation of corrosive species. Besides, the PF_6^- anions enrich in the Helmholtz plane of LCO/electrolyte interface, and promote the formation of robust cathode/electrolyte interphase (CEI) featuring with $LiF/Li_xPO_yF_z/Li_3PO_4$ inorganics and P-containing organics, under the synergy of fluorinated solvents, which significantly inhibits the catalysis of highly oxidative Co^{4+}/O^{n-} ($0<n<2$). Benefited from the reduced corrosive species and reinforced CEI, the layered structure of LCO surface is well-preserved upon long-term cycle, with a highly reversible O3/H1-3 phase transition. Consequently, the LCO||graphite pouch cell exhibits a remarkable capacity retention of 85.7% after 500 cycles in 3.0-4.55 V. This work provides a new insight in developing the advanced functional electrolytes for high-voltage lithium-ion batteries.

Introduction

$LiCoO_2$ (LCO) has long been the indispensable cathode material in consumer electronics fields, mainly due to its high volumetric energy density, and high rate/cycle performances. With the acceleration of lightweight tendency of the new electronic products, the application of LCO cathodes calls for higher cut-off voltage beyond 4.5 V (vs. Li/Li^+, hereafter) to release more reversible specific capacity with significantly enhanced energy density. However, high-voltage (HV) operation can seriously threaten the stability of the LCO/electrolyte interface, which is mainly reflected in the severe interface parasitic reactions derived from the intensively catalytic oxidation activity of Co^{4+}/O^{n-} ($0<n<2$) on LCO surface, and the surface structure degradation originated from the Co/O loss, etc.[1-4] These issues further cause the deteriorated Li^+ diffusion kinetics across the LCO surface, and destroy the reversibility of bulk phase transitions, leading to the crack's formation, and the resultant rapid capacity decay.[5-8] To alleviate the issues, optimizing the interface properties, especially through electrolyte tuning, is the most efficient and low-cost route to stabilize the structure of LCO at high voltage.

As is known, the commercially used electrolytes are usually composed of the cyclic carbonate (such as, ethylene carbonate, EC), linear carbonate (such as, ethyl methyl carbonate, EMC or diethyl carbonate, DEC) solvents, and low concentration $LiPF_6$ salt. However, in most occasions, the combinations between them are pretty hard to tolerate HV operation beyond 4.5 V, showing severe electrochemical decomposition on both LCO cathodes and graphite/Li anodes' interfaces, as depicted in **Fig. S1 (ESI†)**.[9] The continuous oxidation/dehydrogenation of EC/EMC solvents generate detrimental H^+/H_2O, accompanying with CO/CO_2 gas release.[2,10,11] Meanwhile, the increased H^+/H_2O concentration further intensify the decomposition (hydrolysis) of the $LiPF_6$ salt, forming plenty of corrosive species, such as HF, HPO_2F_2, H_2PO_3F, and H_3PO_4, etc.[9,12] These corrosive species cause severe Co dissolution from LCO surface, finally leading to its structure degradation and the formation of fragile cathode/electrolyte interphase (CEI). It is noted that, the Co dissolution from LCO side has a cross effect on the Li metal or graphite anodes, i.e., the Co^{2+} can deposit on the anode sides, and further cause the passivation of anodes.[13] Therefore, enhancing the overall stability of the electrolyte to remove the HF and H_2O, and forming a protective CEI to reduce undesirable interface reactions, are the key breakthroughs to stabilize LCO structure from the aspect of electrolyte tuning.

Compared to the traditional EC solvent, the emerging fluorinated cyclic carbonates (including

fluoroethylene carbonate, FEC, and difluoroethylene carbonate, DFEC, etc.) gradually show their great potential in HV applications due to the enhanced anti-oxidative properties.[14-19] Recently, they have been widely investigated as electrolyte additives or solvents in electrolyte, which can regulate the Li^+ solvation structure, and promote the formation of robust solid electrolyte interphase (SEI) on Li metal or Si/Si-C anodes.[16,20,21] As reported previously, with increased fluorination extents of solvents from EC, FEC to DFEC, the Li^+ desolvation energy from the electrolytes decreases with the promoted Li^+ transport kinetics, finally contributes to the improved low-temperature performance.[18] In addition, the FEC and DFEC are promising reducible sacrificial agents to help reconstruct the robust SEI on anode with a certain amount of LiF, $ROCO_2Li$ and polymeric species, especially utilizing their synergetic effects.[20,22,23] Despite the above insights, the detailed optimization mechanism of FEC/DFEC solvents on enhancing the HV cycle performance of LCO still remains vague, and requires further investigation.

In this work, the optimization mechanism by rational control of electrolyte solvents from EC to FEC/DFEC solvents is systematically explored based on comprehensive characterizations and theoretical simulations. We find that, the enhanced stability of LCO in an anti-oxidative FEC-DFEC based electrolyte is basically attributed to reduced corrosive species and the formation of robust and uniform CEI, which significantly reduce the catalysis of highly oxidative Co^{4+}/O^{n-} ($0<n<2$), and play important roles in stabilizing surface structure as well as enhancing the phase transition reversibility of LCO. Specifically, under the synergy of anti-oxidative and weak-solvated fluorinated solvents, the reaction path of PF_6^- anions in the inner Helmholtz plane of LCO/electrolyte interface is regulated, which reduces the hydrolysis of PF_6^- to form the corrosive species, such as HF, HPO_2F_2, etc., but to promote the formation of robust CEI abundant with $LiF/Li_xPO_yF_z/Li_3PO_4$ inorganics and P-containing organics. As a result, the LCO cathode shows the significantly enhanced rate capability and long-term cycle stability with a high capacity retention of 85.5% after 1000 cycles in LCO||Li cells between 3.0-4.6 V and 85.7% after 500 cycles in LCO||graphite pouch cells between 3.0-4.55 V.

Results and discussion

Electrolyte regulation

Starting with the most basic electrolyte system comprising of commonly used solvents of cyclic and linear carbonates (EC/EMC), given that the DEC is more stable than EMC, and the fluorinated EC

solvents (FEC/DFEC) have the enhanced anti-oxidation properties, five kinds of electrolytes are rationally designed to understand the effects of solvent tuning on the electrochemical stability upon HV operation, as listed in **Table S1 (ESI†)**. As illustrated in linear sweep voltammetry (LSV) results (**Fig. S2, ESI†**), the partial replacement of EMC by DEC can inhibit the drastic oxidative decomposition of electrolyte to a certain extent. Besides, further replacing EC with fluorinated solvents (FEC/DFEC) exhibits extended electrochemical window to higher potential. Therefore, it is necessary to understand the effects of solvent's tuning on its physicochemical properties and resultant cell performances. As reported previously, there always exists an electrical double layer (EDL) between the electrode surface and electrolyte, calling as the Helmholtz plane, which includes the inner Helmholtz plane (IHP) and outer Helmholtz plane (OHP). Generally, the OHP contains Li^+ ions inside the solvation shells, and the IHP contains anions and organic molecules adsorbing on the LCO/electrolyte interface.[2,24,25] Specifically, the difference in solvation structures of OHP will significantly affect the (de)solvation kinetics of Li^+ ions and the chemical species in IHP, finally leading to distinct CEI layer.

We first analyze the interaction between the Li^+ ions and solvents (including EC, FEC, DFEC, etc.) via the density functional theory (DFT). The calculated binding affinity can qualitatively evaluate the interaction strength between the Li^+ ions and solvents.[18] As shown in **Fig. S3a (ESI†)**, the binding affinity values of Li^+-fluorinated solvents are higher than that of Li^+-EC, indicating the weaker solvation strength between Li^+ ions and FEC/DFEC solvents. **Fig. 1a and Fig. S3b (ESI†)** further show the calculated Li^+ solvation energies in a $Li^+[solvents]_4$ solvation structure, and it is clear that the DFEC-derived one is the most prone to release the free Li^+ ions, whether we replace one solvent molecule ($Li^+[EC]_3[DFEC]$) or replace all of them ($Li^+[DFEC]_4$). Besides, the necessary involvement of FEC solvents helps to stabilize Li^+ solvation structure and to regulate electrolytic viscosity to some extent.[26]

The difference in the Li^+-solvents interaction will affect greatly on the coordination of the PF_6^- anions in the solvation structure. In Raman spectra of electrolytes (**Fig. 1b**), the peaks at Raman shift of about 720 and 740 cm^{-1} correspond to the free and solvated PF_6^-, respectively. It can be seen that, the weaker the Li^+-solvents interaction, the higher the intensity of the solvated PF_6^-. In **Fig. 1c and S4a (ESI†)**, the results of Fourier transform infrared spectroscopy (FTIR) also indicate that, less free PF_6^- (840 cm^{-1}) and more solvated PF_6^- (870 cm^{-1}) exist in the fluorinated electrolyte. Besides, in **Fig.**

S4b (ESI†), the up-field shifts of ^{7}Li nuclear magnetic resonance (NMR) spectra in fluorinated electrolytes, which are EC-free and weakly-solvated, further demonstrate the intensive PF_6^--shielding effect on the Li^+ ions, corresponding well to the Raman and FTIR results.[27]

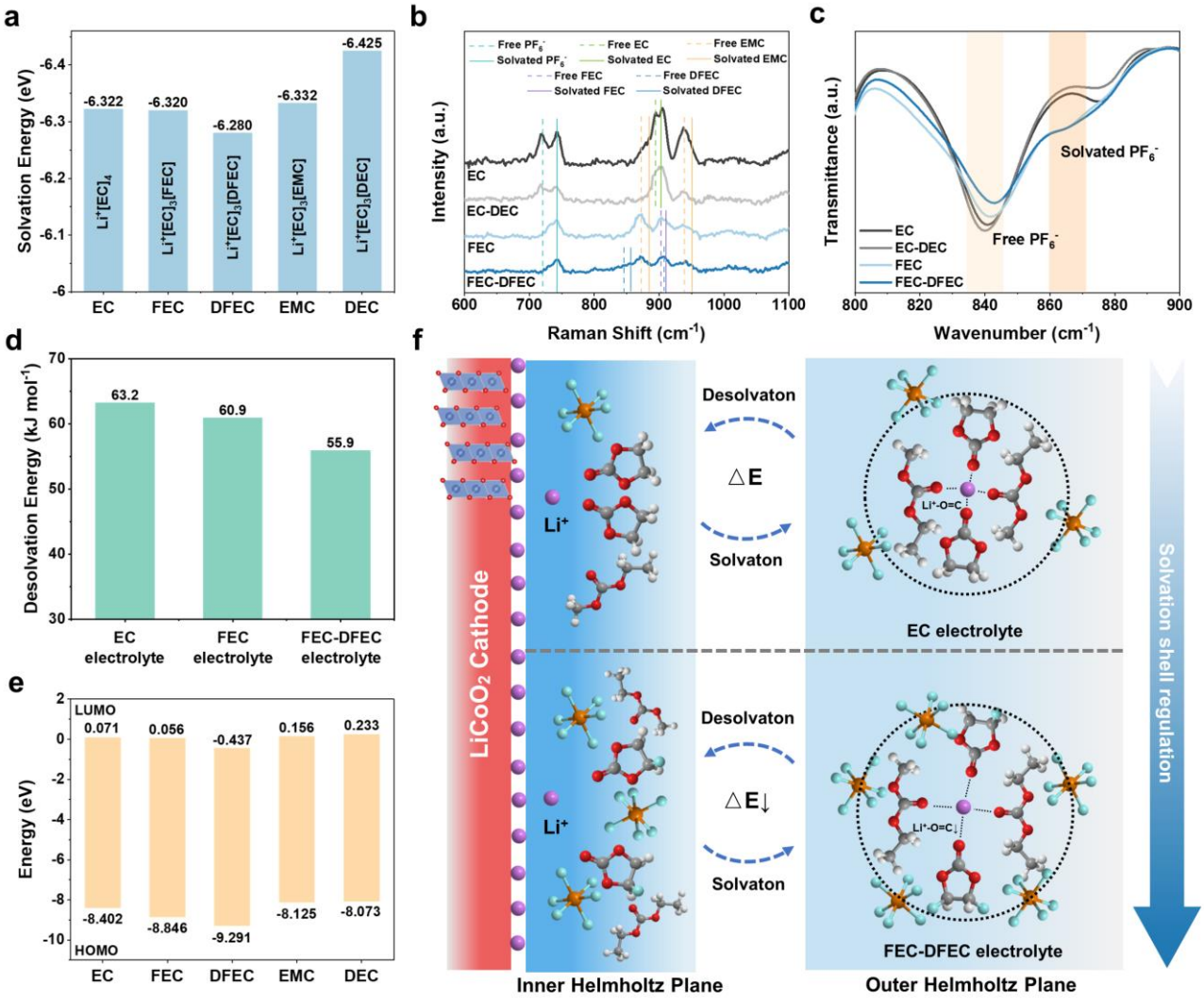

Fig. 1 The influence of electrolyte regulation on Helmholtz Plane. a) Calculated the Li^+ solvation energy in Li^+[solvents]$_4$ solvation structure. b) Raman spectra and c) FTIR spectra of EC, EC-DEC, FEC and FEC-DFEC electrolytes. d) The Li^+ desolvation energy in EC, FEC and FEC-DFEC electrolytes by fitting the R_{ct} of $Li_{0.7}CoO_2$||$Li_{0.7}CoO_2$ symmetric cells obtained under various temperatures with Arrhenius equation. e) Calculated HOMO/LUMO energy of various solvents. f) The schematic diagram of inner and outer Helmholtz Plane regulation in FEC-DFEC electrolyte.

The temperature-dependent electrochemical impedance spectroscopy (EIS) measurements (**Fig. S5, ESI†**) are further applied to quantify the Li^+ desolvation kinetics on the LCO surface in different

electrolyte.[28] We conduct the $Li_{0.7}CoO_2||Li_{0.7}CoO_2$ symmetric cell to exclude the effect of CEI layer and damage to the surface layer structure. The fitted results (**Fig. 1d and Fig. S5, ESI†**) show that the Li^+ desolvation energy in FEC (60.9 kJ mol^{-1}) and FEC-DFEC (55.9 kJ mol^{-1}) electrolytes are obviously lower than that in EC electrolyte (63.2 kJ mol^{-1}), exhibiting the facilitated Li^+ ions (de)solvation kinetics in FEC and FEC-DFEC electrolytes. And the mild increase of the Li^+ desolvation energy in DFEC electrolyte (61.6 kJ mol^{-1}) can be attributed to the synthetical effects by Li^+-solvents/anions interaction, *i.e.*, the weak Li^+–DFEC interaction lead to the significantly enhanced Li^+–PF_6^- interaction, resulting in the increased Li^+ desolvation energy. During the cycle, the de-solvated PF_6^- anions and solvents can gather in IHP to anticipate the interface reactions. The lowest unoccupied molecular orbital (LUMO) and highest occupied molecular orbital (HOMO) energies of the solvents are further calculated via DFT calculations, to reveal potentials of reduction/oxidation stability of organic solvents in IHP/OHP. Both of the HOMO and LUMO energies of DFEC and FEC are lower than EC (**Fig. 1e**), which indicate their enhanced anti-oxidative stability on LCO side and preferential reduction to form initial SEI on Li or graphite side. Furthermore, the HOMO and LUMO energies of various $Li^+[solvents]_4$ solvation structure (**Fig. S6, ESI†**) also indicate that, completely replacing EC solvent with FEC/DFEC solvents can dramatically enhance the anti-oxidative stability and reduction activity of solvation structure.

As summarized in **Fig. 1f**, the introduction of FEC/DFEC solvents can effectively regulate the IHP and OHP, leading to weaker interaction between Li^+ ions and solvents, and more PF_6^- anions participating in the Li^+ solvation sheath. On one hand, in OHP, the lower Li^+ (de)solvation energy ensures a fast Li^+ transport kinetics. On another hand, in IHP, more electrochemically anti-oxidative organic solvents and the PF_6^- anion-dominant interface chemistry significantly promote thte formation of chemo-mechanically stable CEI abundant with inorganic species during cycle, thereby improving the compatibility of regulated electrolyte with LCO at 4.6 V.

Cell performances

The cell performances of the progressively optimized electrolytes are evaluated by assembling LCO||Li cells. The correlated X-ray diffraction (XRD) results of pristine LCO are presented in **Fig. S7 (ESI†)**, showing a pure layered α-$NaFeO_2$ structure with space group of *R-3m*. Transmission electron

microscope (TEM) characterizations and correlated diffraction patterns are further utilized to analyze the surface and bulk structures of LCO (**Fig. S8, ESI†**), both showing the characteristics of layered structure. The initial charge/discharge curves of LCO||Li cells (**Fig. 2a and Fig. S9, ESI†**) indicate that, through regulating the solvents, it exhibits a high reversible discharge capacity of ~220 mA h g^{-1}, and a high initial Coulombic efficiency (ICE) of up to ~96.3% cycling in FEC-DFEC electrolyte, while in EC electrolyte, it exhibits a lower discharge capacity of ~218 mA h g^{-1}, and a ICE of lower than 90%, which are attributed to the reduced interface polarization and optimized interface reaction. The reduced interface polarization can be further confirmed by the cyclic voltammetry (CV) tests in **Fig. 2b and Fig. S10 (ESI†)**. The LCO||Li cells cycled in FEC and FEC-DFEC electrolytes show the much smaller half-peak width and voltage hysteresis than that in EC electrolyte, demonstrating the faster Li^+ transport kinetics.[29] Meanwhile, the lowest leakage current for LCO||Li cells is observed in FEC-DFEC electrolytes, which also indicate the optimized LCO/electrolyte interface with less detrimental side reactions (**Fig. S11, ESI†**). Hence, they display significantly improved rate capability and cycle stability, as shown in **Fig. 2c and Fig. S12 (ESI†)**. At a high current density of 8 C (1 C = 200 mA g^{-1}), the discharge capacities of LCO||Li cells cycled in EC, EC-DEC, FEC and FEC-DFEC electrolytes are 116.6, 131.2, 140.1, and 173.9 mA h g^{-1}, respectively. Meanwhile, after 500 cycles at the rate current of 1 C, the capacity retention of LCO||Li cells in EC, EC-DEC, FEC and FEC-DFEC electrolytes are 37.7%, 61.4%, 83.2% and 92.7%, respectively. Impressively, the LCO||Li cell using FEC-DFEC electrolyte shows a high capacity retention of 85.5% after 1000 cycles at 2 C (**Fig. 2d**), which is among the best reported cycle performances (**Fig. 2e and Table S2, ESI†**). Besides, the comparison of long-term cyclic charge/discharge curves of LCO||Li cells in different electrolytes (**Fig. S13 and S14, ESI†**), and evolution of correlated charge/discharge average voltages upon cycles (**Fig. S15, ESI†**) are further performed, the results suggest the detrimental structural degradation occurring on LCO with severe voltage decay in EC electrolyte. While in FEC-DFEC electrolyte, the charge/discharge curves almost overlap with nearly no change in charge/discharge average voltages within 200 cycles, further confirming the benefiting effects of the solvent regulation. Theoretically, due to the anti-oxidative property of DFEC, the cells in DFEC electrolyte can achieve much better cell performances than that in FEC-DFEC electrolyte. However, as shown in **Fig. S16 (ESI†)**, although the LCO||Li cell using DFEC electrolyte also shows a high capacity retention of 89.6% after 500 cycles at 1 C with significantly reduced voltage decay, the incompatibility between DFEC electrolyte and Li

anode leads to some negative results, including low Coulombic efficiency during cycling and the poor stability of Li||Li symmetric cells, which is attributed to the massive consumption of DFEC on Li anode.[20] In contrast, the FEC-DFEC electrolyte shows better compatibility with Li anode, the correlated Li||Li symmetric cell shows superior plating/striping cycle stability with low over-potential for over 500 h (**Fig. S17, ESI†**). For comparison, the Li||Li symmetric cell with EC electrolyte shows evident fluctuation in voltage hysteresis, and suffers from a sudden short-circuit at about 220 h.

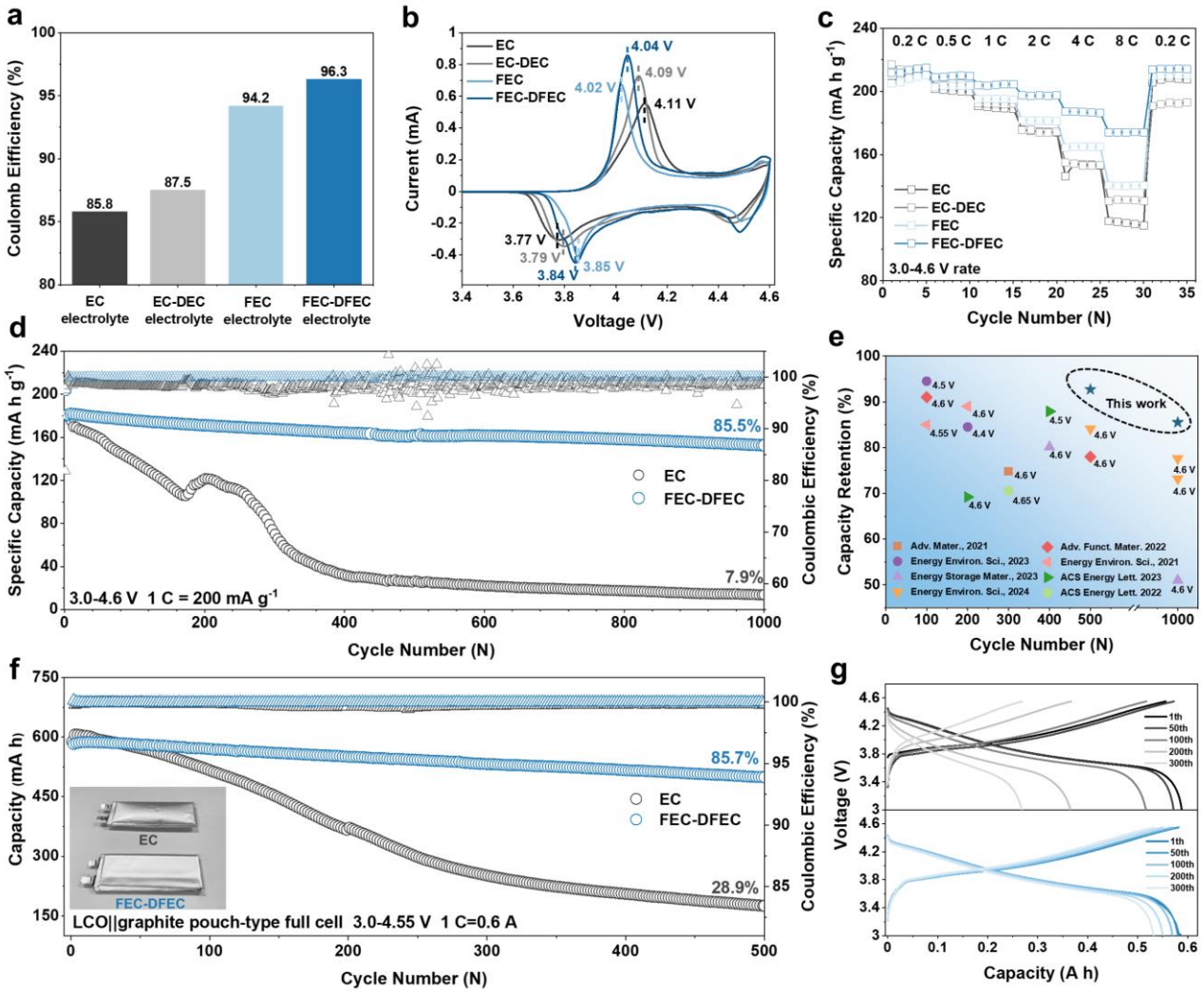

Fig. 2 Cell performances of LCO||Li cells and LCO||graphite pouch cells in differernt electrolytes. a) ICE, b) CV tests and c) rate performances of LCO||Li half cells in EC, EC-DEC, FEC, FEC-DFEC electrolytes within voltage range of 3.0-4.6 V. d) Cycle performance of LCO||Li half cells in EC and FEC-DFEC electrolytes within the voltage range of 3.0-4.6 V, at the current of 2 C. e) Comparison of cell performances of recently reported electrolyte regulation for LCO cathodes at room temperature. f) Cycle performance of LCO||graphite pouch type full cell within a voltage range of 3.0-4.55 V at 1 C

in EC, FEC-DFEC electrolytes and the digital photograph of pouch type full cell after 500 cycles. g) The corresponding charge and discharge curves at different cycles for LCO||graphite pouch cell.

The LCO||graphite pouch-type cells (with capacity of about 0.6 A h) are further fabricated to evaluate the feasibility of the designed FEC-DFEC electrolyte. As presented in **Fig. 2f, g**, the LCO||graphite cell with FEC-DFEC electrolyte presents an excellent cycle stability with a high capacity retention of 85.7% after 500 cycles in 3.0-4.55 V at 1 C without visible swelling detected. As a comparison, the LCO||graphite full cell with the EC electrolyte shows a rapid capacity decay with obvious swelling upon cycles, indicating the severe electrolyte decomposition and interface side reactions. Besides, benefiting from the promoted Li^+ transport kinetics of FEC-DFEC electrolyte, the LCO||graphite cell shows outstanding low-temperature performance with a high capacity retention of 88.2% at -20 ℃ comparing with that at 25 ℃ (**Fig. S18, ESI†**).

Reduced interface side reaction

The optimized LCO/electrolyte interface reaction is the origin of realizing its better electrochemical performances at 4.6 V. Herein, several *in-situ* characterizations are combined to explore the optimization mechanism behind. In **Fig. 3a**, the *in-situ* Raman spectra of LCO||Li cells with EC and FEC-DFEC electrolytes are obtained for the initial two cycles in 3.0-4.6 V, and the correlated CV curves are shown in **Fig. S19 (ESI†)**. The characteristic Raman peaks of LCO, locating at the Raman shifts of 485 and 595 cm^{-1}, can be assigned to O-Co-O bending mode (E_g) and Co-O stretching mode (A_{1g}), respectively.[30,31] It is noted that, for EC electrolyte, when the voltage is beyond 4.2 V, the E_g and A_{1g} peaks disappear in the 1st cycle, and their intensity decreases significantly in the 2nd cycle, mainly attributing to the breakage of Co-O bonds, which is induced by the severe interface side reactions between the highly oxidative Co^{4+}/O^{n-} ($0<n<2$) and the EC electrolyte. This finally results in the structure degradation from "layered to spinel/rocksalt" on the LCO surface, since there appears a new peak at 670 cm^{-1} at Raman spectra after cycles (**Fig. S20, ESI†**).[30,32] In contrast, in FEC-DFEC electrolyte, the E_g and A_{1g} peaks remain constant during cycle even charging to a high voltage of 4.6 V, indicating the stabilized Co-O bonds on LCO surface. Besides, there is no signals observed at 670 cm^{-1} after cycles, illustrating the stabilized layered phase on LCO surface.

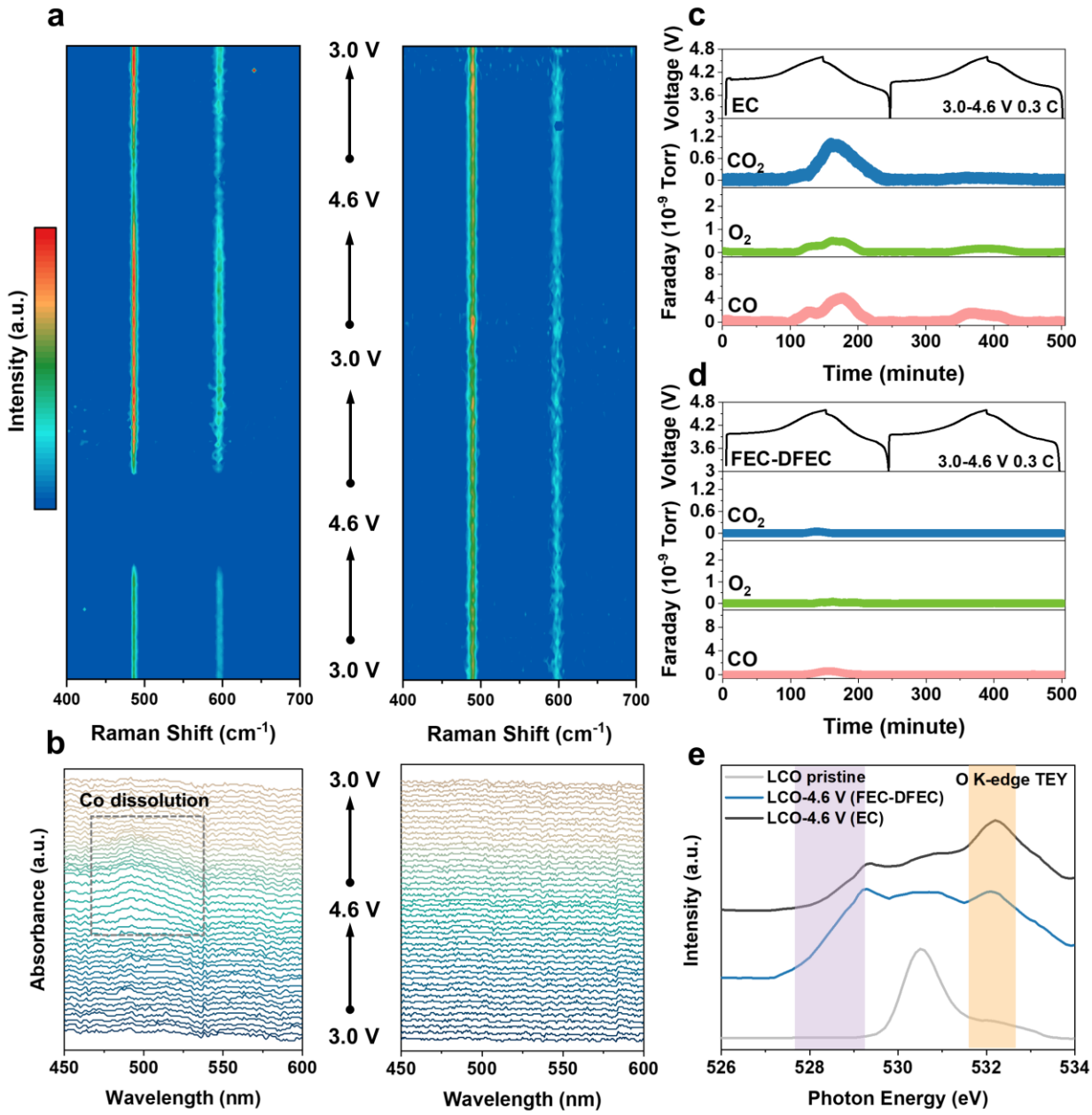

Fig. 3 Characterizations of LCO/electrolyte interface side reaction. a) The *in-situ* Raman spectra of LCO||Li half cells in EC, and FEC-DFEC electrolytes within a voltage range of 3.0-4.6 V at a constant voltage scanning of 0.2 mV s^{-1}. b) The *in-situ* UV-Vis characterization within a voltage range of 3.0-4.6 V at a constant voltage scanning of 0.2 mV s^{-1}. The *in-situ* DEMS tests of LCO||Li cells in c) EC and d) FEC-DFEC electrolytes within a voltage range of 3.0-4.6 V, e) O K-edge spectra of TEY mode from sXAS measurements of pristine LCO and LCO with two types of electrolytes at 4.6 V after 10 cycles within a voltage range of 3.0-4.6 V.

Then, the *in-situ* ultraviolet-visible spectrophotometry (UV-Vis) is adopted to understand the chemical degradation of LCO.[33] As observed in **Fig. 3b**, there are obvious signals of Co^{2+} dissolution near the wavelength of ~500 nm upon charging LCO to 4.6 V in EC electrolyte, which can not be detected for the LCO cycled in FEC-DFEC electrolyte and can be confirmed by the inductively coupled plasma-optical emission spectroscopy (ICP-OES) tests (**Fig. S21, ESI†**).[34] Since the low-valence Co ion's dissolution from LCO surface is regarded as the result of HF corrosion and oxygen loss, it is reasonable to hypothesize that the modified solvation chemistry in FEC-DFEC electrolyte is capable to construct a protective CEI with the inhibited generation of corrosive HF species, and reduced interface side reactions.

The interface reaction can be further detected via *in-situ* differential electrochemical mass spectrometry (DEMS) tests (**Fig. 3c, d**), in which the gas release from the LCO||Li cells is presented for the initial two cycles in 3.0-4.6 V. For LCO||Li cell in EC electrolyte, massive contents of CO_2, O_2 and CO release in the high-potential range during the first cycle, which continuously proceeds in the second cycle. The obvious gas release is attributed to the following aspects, i.e., i) the oxidation of EC and EMC solvents is aggravated by the highly oxidative Co^{4+}/O^{n-} ($0<n<2$), and ii) HF constantly attacks the LCO surface upon charging, deteriorating the surface O loss. As a comparison, there is nearly no gas release observed in FEC-DFEC electrolyte during the initial cycles, indicating the optimized interface reaction by effective electrolyte regulation. Furthermore, the soft X-ray absorption spectroscopy (sXAS) is applied to identify the reinforced structure stability by the solvent regulation. **Fig. 3e** compares the O K-edge spectra (TEY mode) results of pristine LCO, LCO at the charged state (at 4.6 V, after 10 cycles) in EC and FEC-DFEC electrolytes, respectively. For pristine LCO, the peak locating at the photon energy of 530.5 eV corresponds to the hybridization of Co^{3+} (e^*_g) - O 2p. For LCO charging to 4.6 V, the peaks locating at photon energy of 529 eV and 527 eV emerge, corresponding to hybridization of Co^{4+} (e^*_g) - O 2p and Co^{4+} (t_{2g}) - O 2p, indicating a much more remarkably ascending of Co valence in the surface for LCO in FEC-DFEC electrolytes compared with EC electrolyte.[35] Meanwhile, the peaks locating at ~532 eV also arise obviously, illustrating the formation of low-valence Co (such as Co_3O_4 or CoO) or Li_2CO_3 on LCO surface, and the relative peak intensity is obviously higher for LCO at 4.6 V in EC electrolyte than that in FEC-DFEC electrolyte.[36,37] We further conduct the (cryogenic transmission electron microscopy) cryo-TEM measurements to characterize the surface region of LCO in different electrolyte after 10 cycles in 3.0-4.6 V. **Fig. S22**

(ESI†) indicates that, uneven surface structure damage and CEI layer distribute on the LCO, indicating serious interface side reactions occur on the LCO in EC electrolyte, while LCO in FEC-DFEC electrolyte exhibits intact particle and thin CEI layer with a thickness of lower than 5 nm. In summary, the solvents' decomposition induced by oxidative Co^{4+}/O^{n-} ($0<n<2$) and surface structure degradation of LCO with severe Co/O loss can be largely alleviated by using FEC-DFEC electrolyte.

Formation of robust CEI

As discussed above, the regulation of IHP and progressively construction of CEI layer on LCO surface in FEC-DFEC electrolyte are responsible for the reduced interface side reactions, thus it is critical to dissect its structure and composition to understand the optimization mechanism. Herein, the structure electrochemistry in LCO/electrolyte interface is firstly characterized by *in-situ* EIS, as shown in **Fig. S23a, b (ESI†)**. The EIS curves can be fitted and resolved to obtain two significant parameters (**Fig. S23c, d, ESI†**), i.e., the surface film resistance (R_{sf}) referring to property of CEI/SEI, and the charge transfer resistance (R_{ct}) referring to the property of LCO surface after 10 cycles.[38] As observed, the FEC-DFEC electrolyte leads to more stable CEI/SEI formation due to the slight fluctuation of R_{sf} values during cycle, and better surface Li^+ transport kinetics with remarkably decreased R_{ct} values. **Fig. 4a-d, Fig. S24 and S25 (ESI†)** compare the cryo-TEM morphologies of LCO in different particles after 100 cycles in EC and FEC-DFEC electrolytes, respectively. Upon cycles, a loose and non-uniform CEI is formed on LCO surface in EC electrolyte (**Fig. 4a, b**), while a dense and homogeneous CEI with a thickness of 20 nm is formed in FEC-DFEC electrolyte (**Fig. 4c, d**). In addition, as analyzed from the the fast Fourier transform (FFT), the CEI formed in EC electrolyte contains LiF and some amorphous species, while for the CEI formed in FEC-DFEC electrolyte, there are large amounts of inorganic species, including the Li_3PO_4, LiF and Li_2CO_3, etc.

The *in-depth* X-ray photoelectron spectroscopy (XPS) is further applied to characterize the chemical compositions of CEI on LCO and correlated SEI on Li anode after 100 cycles. In **Fig. S26 (ESI†)**, the analyses of C 1s, O 1s, F 1s, P 2p, and Li 1s XPS results are performed, and the illustration of the fitted results are clarified in detail in **ESI†**. Generally, in EC electrolyte, the CEI on LCO surface contains the PF_6^- decomposition-derived $LiF/Li_xPO_yF_z$ inorganics and solvents decomposition-derived organics, mainly due to the expense of forming more corrosive species (**Fig. S26, ESI†**). And, the SEI

on Li metal has a similar composition accompanied with obvious Co deposition, as shown in the **Fig. S27 and S28 (ESI†)**. The characters of CEI/SEI in FEC-DFEC electrolyte based on XPS results can be illustrated as follows. First, there is no visible signal of Co detected on surface of the cycled Li anode in FEC-DFEC electrolyte, indicating the reduced formation of corrosive species and cross effect of Co upon cycles. Second, it shows a lower signal peak of Co-O lattice in O 1s spectra, indicating the well-covered CEI to protect the LCO surface from corrosion. Third, there appears a new peak at 283.5 eV in C 1s spectra, referring to the formation of organic species due to the "cross effect" of the decomposition of FEC/DFEC solvents from the anode side, which will be discussed subsequently.[39-41] Fourth, due to the more PF_6^- ions participating in Li^+ solvation structure, there exists more LiF inorganics, while the content of P-containing species also increases with few Co dissoultion (including $Li_xPO_yF_z$, $OPF_x(OR)_y$ and phosphate (Li_3PO_4, $OP(OR)_3$) etc., in which the R represents the alkyl chain), resulting in the uniform and robust CEI in FEC-DFEC electrolyte.[42, 43] Thus, based on the FEC-DFEC electrolyte, both the CEI on LCO side and the SEI on Li anode side are robust and uniform, which is vital for the enhanced cell performances under HV operation.

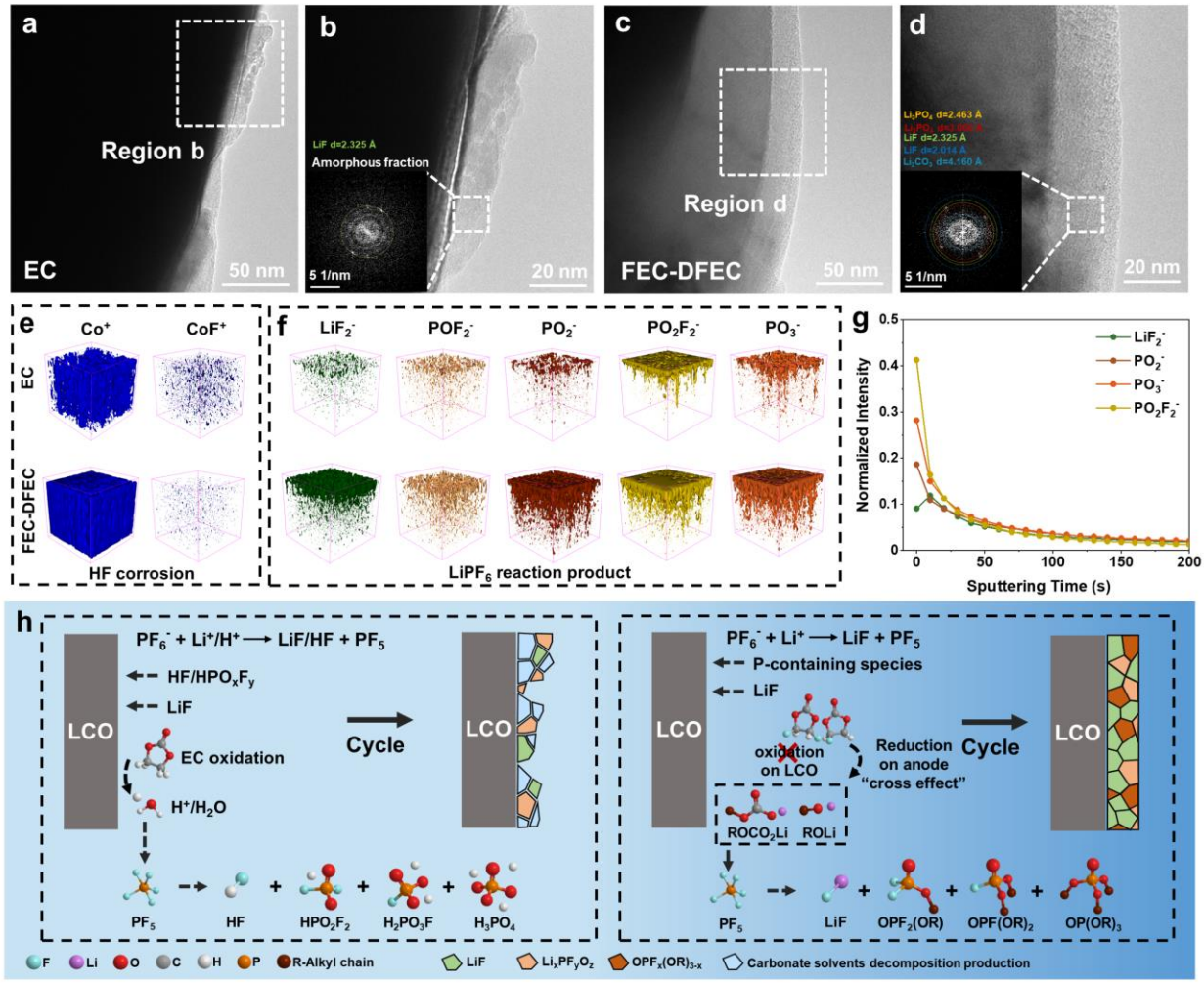

Fig. 4 Morphology and composition analyses of LCO CEI layer. Cryo-TEM characterizations of LCO CEI layer and FFT analysis after 100 cycles of LCO||Li cells in a,b) EC and c,d) FEC-DFEC electrolytes within a voltage range of 3.0-4.6 V at 1 C. e,f) The 3D reconstruction of diverse kinds of secondary-ion fragments for the LCO/electrolyte interface in EC and FEC-DFEC electrolyte. g) The distribution of LiF_2^-, POF_2^-, PO_2^-, PO_3^-, and $PO_2F_2^-$ species in CEI layer from outside to inside. h) Schematic of the LCO CEI formation during the cycle in EC and FEC-DFEC electrolytes.

To further understand the mechanism of robust CEI formation, the spatial distribution of species in CEI layers on LCO surface are investigated by time-of-flight secondary ion mass spectrometry (TOF-SIMS) measurements. **Fig. 4e** shows a seriously corroded LCO surface with Co loss and generating Co-F species in EC electrolyte, while in FEC-DFEC electrolyte, the LCO surface is well-maintained with nearly no visible signs of corrosion and Co-F species, which indicates the inhibition of corrosive species (such as HF, HPO_xF_y, etc.) in FEC-DFEC electrolyte. However, **Fig. 4f and Fig.**

S29 (ESI†) display the more uniform and robust spatial distributions of the LiF_2^-, POF_2^-, PO_2^-, $PO_2F_2^-$, and PO_3^- species in CEI formed in FEC-DFEC electrolyte than that formed in EC electrolyte. Combining the XPS results (**Fig. S26, ESI†**), it suggests that, in FEC/DFEC electrolyte, there is more PF_6^- anions participating in the Li^+ solvation structure, leading to the different reaction pathway in comparison with hydrolysis reaction in EC electrolyte, thus avoids the formation of corrosive species but promotes the generation of P-O species. **Fig. 4g** show the variations in the distribution of CEI products from surface to inside. It illustrates that, the LiF_2^- seems to locate in the inner layer of CEI, while the POF_2^-, PO_2^-, $PO_2F_2^-$, and PO_3^- species tend to locate in the outer layer of CEI. That is to say, upon cycles, the PF_6^- anions enriches in the IHP region of LCO/electrolyte interface, and tends to preferentially deposit on the surface of LCO, forming the PF_5 and inner LiF species. Then, the PF_5 species further reacts with the reduction products of FEC/DFEC (i.e. lithium alkyl carbonates ($ROCO_2Li$), lithium alkoxide (ROLi), as shown in **Fig. S30, ESI†**), forming more P-containing organic species in the outer layer (i.e., $OPF_x(OR)_y$ and $OP(OR)_3$), corresponding to the P/F/O-containing species in TOF-SIMS results.[41,44-47] Also, the $Li_xPO_yF_z$/Li_3PO_4 inorganics shown in XPS and cryo-TEM results are related to the further decomposition of $OPF_x(OR)_y$ and $OP(OR)_3$ species.

Furthermore, we assemble the LCO||$Li_4Ti_5O_{12}$ (LTO) full cells to confirm the "cross-effect" of reduction products of FEC/DFEC from the Li/graphite anode (**Fig. S31, ESI†**). The XPS spectra of the LCO cathode electrode with different etching time after 50 cycles of LCO||LTO cells indicate that both Li-O-C peak (located at 283.5 eV in C 1s spectra) and P-O peak (located at 134 eV in P 2p spectra) are absent on the LCO (**Fig. S32, ESI†**). Besides, cryo-TEM images and FFT result on different LCO particles (**Fig. S33, ESI†**) show that, plenty of LiF nano particles deposit on the LCO surface, and the near-surface region of LCO still remains a pure layered phase. The enrichment of LiF component and stable surface structure of LCO can be attributed to the PF_6^- anions and anti-oxidative FEC/DFEC solvents-dominant interface chemistry in IHP of LCO in FEC-DFEC electrolyte, which is consistent with the LCO cycled in LCO||Li cells. However, the lack of P-O XPS signal and Li_3PO_4 inorganic component can be attributed to the flat and high potential plateau of LTO anode (at about 1.55 V vs. Li^+/Li), which inhibit the FEC/DFEC reduction on the anode side to some extent, and further affect the CEI evolution process. Additionally, the poor cyclic stability of LCO||LTO cells may be attributed to the catalytic activity of LTO surface, which can induce some interface side reaction accompanying with gas release.[48,49]

Combing the cryo-TEM, XPS, TOF-SIMS results, the mechanism of forming a robust CEI on LCO surface can be fully illustrated in **Fig. 4h**. In EC electrolyte, upon cycles, the oxidation of EC solvents leads to the generation of H_2O/H^+, promotes the hydrolysis of PF_6^- anions to form some corrosive species (such as, HF, HPO_xF_y, etc.). These corrosive species not only cause the surface structure degradation, but also obstruct the formation of well-protective CEI on LCO surface. As a result, a loose and non-uniform CEI is formed on LCO surface. In contrast, in FEC-DFEC electrolyte, upon cycles, the solvents are much stable to resist the oxidation on LCO surface. Besides, in IHP region of LCO/electrolyte interface, the PF_6^- anions are more concentrated due to the regulation of the solvation chemistry, which promotes more deposition of $LiF/Li_xPO_yF_z/Li_3PO_4$ inorganics and P-containing organics in CEI, under the synergy of reduction products of FEC/DFEC. Consequently, the CEI formed in FEC-DFEC electrolyte presents a chemo-mechanically stable feature, which can effectively reduce the Co^{4+}/O^{n-} ($0<n<2$) induced interface side reaction and surface degradation of LCO, especially upon long-term cycles.

Long-term characterizations

As discussed above, a robust CEI with high chemo-mechanical stability and better Li^+ ions transport kinetics is achieved in FEC-DFEC electrolyte, which enhances the reversibility of bulk phase transition in return, and finally enables the long-term cycle stability of LCO. Herein, the dQ/dV curves and *in-situ* XRD patterns are utilized to confirm this perspective. In **Fig. 5a, b**, the redox peaks at potential ranges of 3.9-4.0 V and 4.5-4.6 V in dQ/dV curves represent the O3/O3' and O3'/H1-3 phase transitions, respectively, in which, the latter peaks correlate to the sliding of O-Co-O layer.[6,50] In EC electrolyte, the phase transition reversibility of LCO is not satisfactory, i.e., as cycle proceed, the potential difference between the oxidation and reduction peaks increases gradually for O3/O3' phase transitions, and vanishes for O3'/H1-3 phase transitions after 300 cycles. In contrast, the LCO cycled in FEC-DFEC electrolyte exhibits highly reversible phase transitions, showing a stabilized Li^+ (de)intercalation from bulk LCO, which is due to the reduced surface degradation and the optimized CEI.

The *in-situ* XRD patterns are employed to further probe the influence of electrolyte regulation on the phase transition of LCO (**Fig. 5c, d**). When charged to voltages beyond 4.5 V, the LCO in EC

electrolyte shows a more obvious O3'/H1-3 phase transition than that in FEC-DFEC electrolyte, as characterized by the peak separation of (003) and (101) peaks. Furthermore, when charged to 4.6 V, the (003) peaks of LCO can be divided into three peaks, i.e. O3', O3'/H1-3 (a transition state from O3' to H1-3) and H1-3.[35,51] For LCO in FEC-DFEC electrolyte, qualitatively, the percentages of the O3', O3'/H1-3, and H1-3 are 33%, 52%, and 15% in the 1st cycle, and 32%, 55%, and 13% in the 2nd cycle, respectively. For LCO in EC electrolyte, the percentages of the O3', O3'/H1-3, and H1-3 are 6%, 80%, and 14% in the 1st cycle, and 6%, 50%, and 44% in the 2nd cycle, respectively. The above results demonstrate that, in FEC/DFEC electrolyte, at fully charged state, the LCO contains more O3' phase in FEC-DFEC electrolyte, indicating the reduced slippage of O-Co-O layers. And we consider that, the origin of higher degree of the O3/H1-3 phase transition in EC electrolyte during the initial two cycles is due to the formation of a thin surface spinel phase, with a thickness of about 2-5 nm (**Fig. S34a,b, ESI†**), which is attributed to the interface reactions between LCO surface and EC electrolyte in the 1st charging process. As a result, the polarization of LCO electrode can be reduced to a certain extent, resulting in more Li^+ extracting from LCO upon the activation process in the initial two cycle.[52] On the contrary, due to the regulated interface stability of LCO in FEC-DFEC electrolyte, there is no activation process on LCO surface, which remain layered structure at 4.6 V (**Fig. S34c,d, ESI†**). After 100 cycles, the layered structure of LCO is still well-maintained in FEC-DFEC electrolyte (**Fig. S35, ESI†**). Additionally, the worse cycle life of LCO in EC electrolyte can hardly be related to the higher delithiation depth of LCO in the 1st and 2nd charging process, but is closely related to the severe surface structure deterioration due to the accumulated corrosive species in the LCO/electrolyte interface, and the formation of non-protective CEI in long-term cycles (**Fig.4, Fig. S22 and Fig. S26, ESI†**).

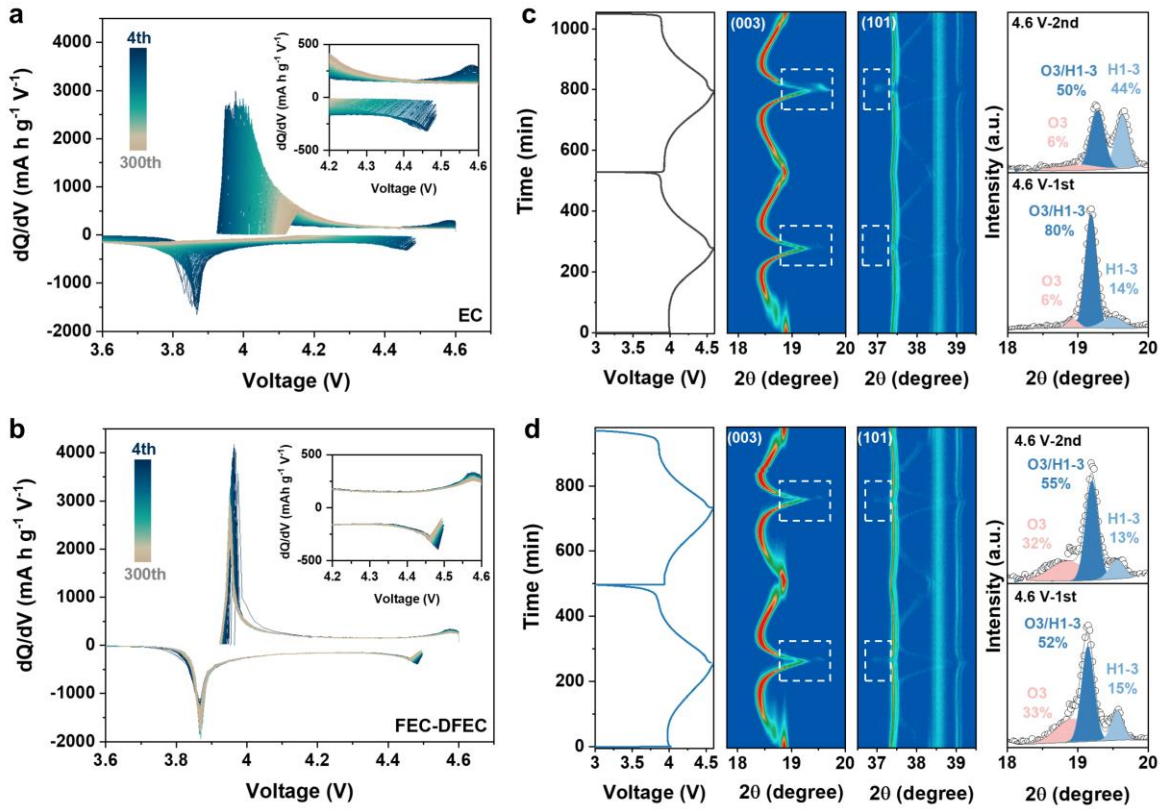

Fig. 5 The influence of electrolyte regulation on the phase transition of LCO. The dQ/dV curves during the cycling of LCO||Li cells in a) EC and b) FEC-DFEC electrolytes in the voltage range of 3.0-4.6 V at 1 C. The *in-situ* XRD measurements and the (003) peak resolving of LCO at 4.6 V in c) EC and d) FEC-DFEC electrolytes in the voltage range of 3.0-4.6 V at 0.25 C.

To further probe the influence of solvents' regulation on surface degradation of LCO upon long-term cycles, the galvanostatic intermittent titration technique (GITT), EIS, SEM and TEM characterizations are performed. As observed in **Fig. S36 (ESI†)**, according to GITT curves, the calculated diffusion coefficient of Li^+ (D_{Li+}) for LCO in FEC-DFEC electrolyte after 100 cycles is significantly higher than that in EC electrolyte. This reinforced and stabilized D_{Li+} value for LCO in FEC-DFEC electrolyte is mainly attributed to the reduced surface degradation, thereby promoting faster Li^+ diffusion kinetics. **Fig. S37a-c (ESI†)**

presents the EIS measurements of LCO after different cycles, and the fitted results of R_{sf} and R_{ct}, in EC and FEC-DFEC electrolytes.[53] Particularly, after 100 cycles, the R_{ct} value for LCO in FEC-DFEC electrolyte is only 300 Ω, far below that of 2300 Ω in in EC electrolyte, demonstrating a much better Li^+ transport kinetics across the stable surface structure. Then, the distribution of relaxation

times (DRT) is further applied to analyze the R_{CEI} and R_{SEI}, which can decouple the intertwined electrochemical steps by capturing their time characteristics (**Fig. S37d, ESI†**). It is noted that, R_{SEI} and R_{CEI} both show increased signal intensity and shift to larger relaxation time τ in EC electrolyte, demonstrating the sluggish Li^+ transport through SEI and CEI due to severe interface side reaction, while for FEC-DFEC electrolyte, the R_{SEI} hold steady and R_{CEI} show decrease signal intensity and shift to lower relaxation time τ, which suggests stable SEI layer and progressively optimized CEI layer (**Fig. 4c**).[54,55]

The cyclic microstructural changes of LCO in different electrolytes are directly observed by SEM and cross-section TEM. As shown in **Fig. S38 and S39 (ESI†)**, after cycles, obvious cracks across the overall LCO particles can be observed in EC electrolyte, while there is no visible crack observed in FEC-DFEC electrolyte, which can be attributed to the following aspects, i) the robust and uniform CEI on LCO surface enables the steady Li^+ (de)intercalation from LCO bulk, ii) the comprehensive result of surface structure stabilization and enhanced phase transition reversibility. In **Fig. 6a**, **b**, the surface structure analyses via TEM and the correlated diffraction patterns are performed. As observed, the LCO surface cycled in EC electrolyte shows an obvious spinel layer with a thickness of about 15 nm, and its subsurface region exhibits a hybrid of layered and spinel phases, indicating the serious irreversible phase transitions. In contrast, FEC-DFEC electrolyte leads to well-preserved layered structure of LCO in both the surface and subsurface regions, illustrating the stabilization of LCO surface for better Li^+ diffusion with more reversible capacity delivery. As reported previously, the formation of thick surface spinel phase is mainly attributed to the O loss at HV, leading to high R_{ct} of cycled LCO in EC electrolyte. Besides, in **Fig. 6c**, **d**, the selected area electron diffraction (SAED) patterns are further applied to revel the surface structure of LCO, in a more macroscopic field with a circular area of 150 nm in diameter. The results show an obvious spinel phase existing in surface region of LCO in EC electrolyte, while in FEC-DFEC electrolyte, the LCO surface shows a pure layer phase structure.

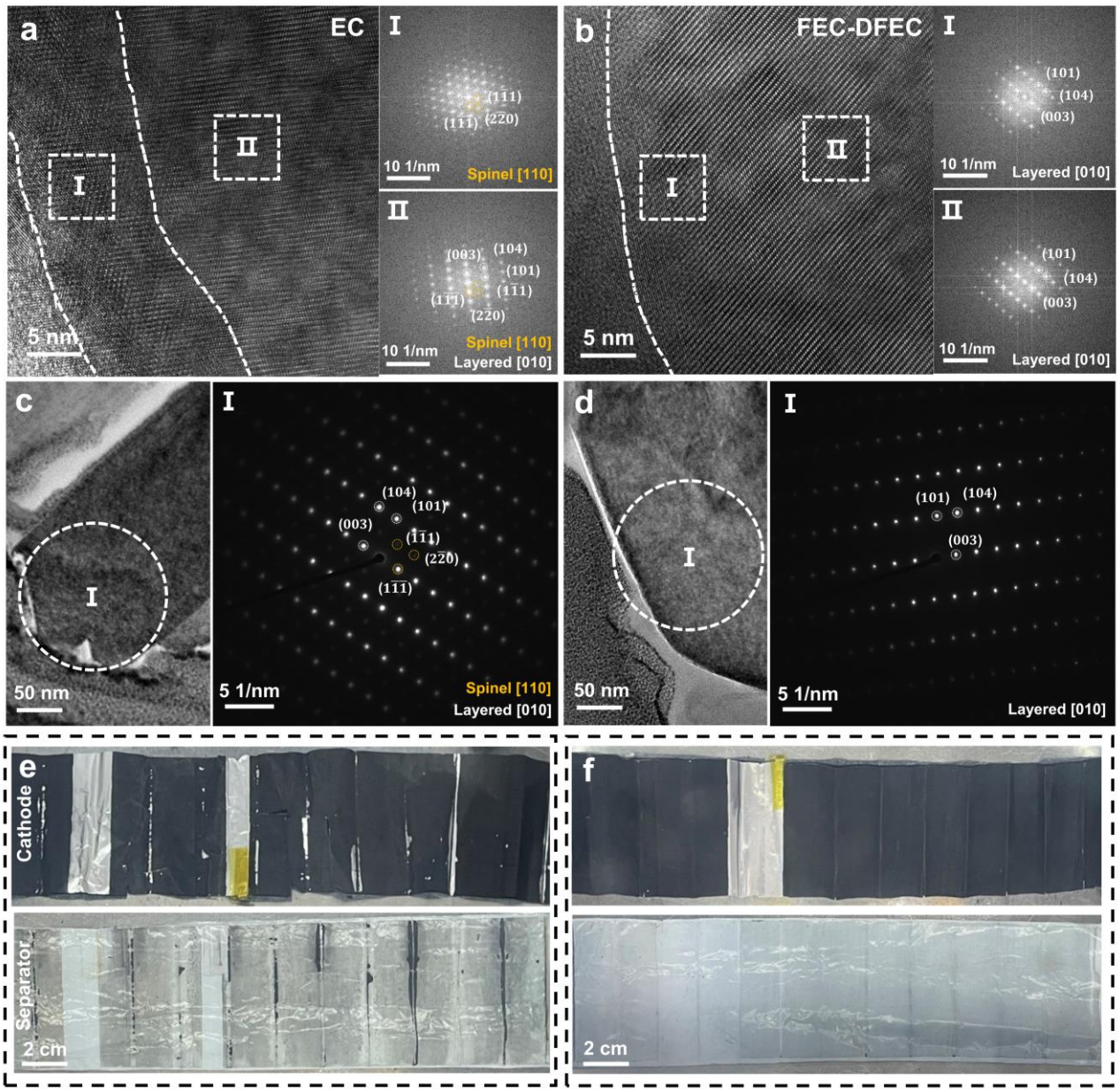

Fig. 6 Long-term characterizations. TEM and corresponding FFT results of LCO after 100 cycles of LCO||Li cells in a) EC and b) FEC-DFEC electrolytes in the voltage range of 3.0-4.6 V at 1 C, and corresponding large-scale TEM and SAED results of LCO in c) EC and d) FEC-DFEC electrolytes. The digital photograph of the positive plate and separator of disassembled LCO||graphite pouch type full cells after 500 cycles in e) EC and f) FEC-DFEC electrolytes within a voltage range of 3.0-4.55 V at 1 C.

As discussed above, the stabilization of LCO is originated from the well-protective CEI layer with significantly reduced corrosive species. To confirm this inference, the LCO||graphite pouch cell after 500 cycles in 3.0-4.55 V is disassembled, and **Fig. 6e, f** show the digital photographs of the LCO

electrodes and separators in two electrolytes. We observe that, in EC electrolyte, the LCO electrode is severely damaged with the active slurry detaching from the Al foils, and the separator is also seriously contaminated by the Co dissolution and severe side reactions, due to the long-term corrosion from corrosive species. In contrast, in FEC-DFEC electrolyte, the LCO electrode maintains its pristine state, and the separator is clean and smooth, indicating much lesser corrosive issues. Further XPS analyses are employed to characterize the LCO electrode and graphite anode of pouch cells, as shown in **Fig. S40 and S41 (ESI†)**. In EC electrolyte, $Li_xPO_yF_z$ species exist in the CEI of LCO due to the hydrolysis of $LiPF_6$, and more Co deposits exist on graphite anode due to the Co dissolution from LCO. However, in FEC-DFEC electrolyte, more LiF and P-containing species are observed on the interface of LCO, with no Co dissolution exist on graphite anode, mainly due to the reduced corrosive species via solvent regulation.

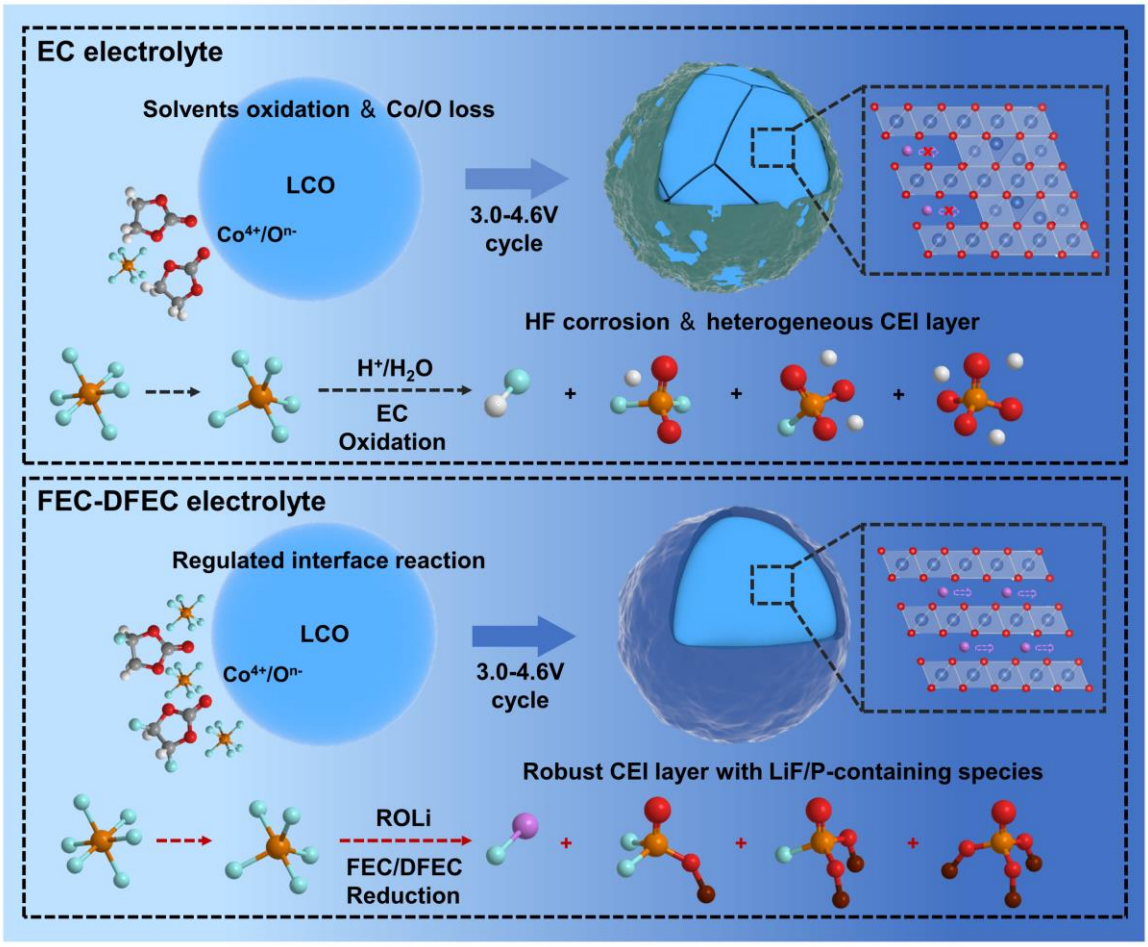

Fig. 7. The mechanism schematic diagram of stabilizing $LiCoO_2$ at 4.6 V in FEC-DFEC electrolyte.

Above all, the stabilization mechanism of LCO in FEC-DFEC electrolyte is illustrated in **Fig. 7**.

In EC electrolyte, upon cycle, the dehydrogenation/oxidation of EC solvents in LCO/electrolyte interface leads to the formation of H_2O/H^+, and subsequently, the hydrolysis of PF_6^- to produce massive corrosive species, such as HF, HPF_2O_2, etc. These corrosive species not only cause the surface degradation via promoting Co/O loss from LCO surface, but also obstruct the formation of well-protective CEI. After long-term cycles, LCO suffers severe surface structure degradation, which seriously blocks the Li^+ transport across the LCO surface, thus leading to a rapid capacity decay. As a comparison, in FEC-DFEC electrolyte, the interface side reaction induced by oxidative Co^{4+}/O^{n-} and the generation of corrosive species are greatly inhibited due to the solvents' regulation, in which the PF_6^- anions enrich and react in the IHP region of LCO/electrolyte interface, promote the formation of uniform and robust CEI, which further protect the integrity of LCO with steady Li^+ ions transport kinetics, and ensure the reversibility of bulk phase transition. Consequently, the LCO exhibits both the enhanced cycle and rate performances in designed FEC-DFEC electrolyte.

Furthermore, we summarize the synthesis technology of fluorine containing carbonates (**Table S3, ESI†**), and recycle technology of used electrolyte (**Table S4, ESI†**), to discuss the feasibility of wide application of using such electrolytes with high concentration fluorinated solvents.[56,57] We believe that, with the development of advanced synthesis methods of FEC/DFEC, i.e. development of high performance, low-cost catalyst, and advanced purification technology of halogen exchange reaction method, or the industrialization of electrochemical fluorination method, combining with the maturity of electrolyte recycling technology, the price of fluorine containing carbonates will continue to decrease (**Fig. S42, ESI†**).[58-60] Additionally, the demand for high-voltage and high-performance electrolytes in the market will continue to grow in the future, which will inevitably push more capital, talent, and resources to gather in the links of research, production, and recycling of high-voltage electrolytes. Thus, we expect that, it is possible to use fluorinated solvents electrolytes in a large-scale, low-cost and environmental-friendly way.

Conclusions

In summary, this work provides a new insight to understand the optimization effect of solvent's regulation. In traditional EC electrolyte, the structure degradation of LCO upon cycle at 4.6 V (vs. Li/Li^+) is mainly originated from severe surface Co/O loss induced by the corrosive species. Replacing

the unstable EC solvent to the FEC/DFEC solvents can effectively regulate the Li^+ solvation structures, comprising of anti-oxidative fluorinated solvents and highly coordinated PF_6^- anions. This optimized electrolyte solvation structure leads to modified interface chemistry of PF_6^- anions, constructing a robust and uniform CEI and reducing the generation of corrosive species, ensuring the well-maintained layered structure of LCO and reversibility of bulk phase transition upon long-term cycles. As a result, the LCO cathode shows the significantly enhanced rate capability and long-term cycle stability at a high cut-off voltage of 4.6 V, with a high capacity retention of 85.5% after 1000 cycles in LCO||Li cells and 85.7% after 500 cycles in LCO||graphite pouch cells.

Author Contributions

H. R. and G. Z. contributed equally to this work. F. P., Q. Z. M. L. and G. Z. proposed and designed the project. H. R. performed electrochemical measurements and carried out characterizations. H. R. and Y. L. conducted and processed TOF-SIMS and XPS measurements. H. R. and S. C. conducted and processed Raman and UV measurements. H. R., H. Y. and J. F. performed the fabrication and performance testing of the pouch cells. H. R. and X. W. conducted the *in-situ* XRD measurements. M. Z. conducted the theoretical calculation. H. R., W. H. and W. Z. conducted and processed the TEM measurements. G. Z., T. L. and L. Y. commented on electrolyte formulations. All authors discussed the results and revised or commented on the manuscript.

Acknowledgements

This work is financially supported by the National Natural Science Foundation of China (52102201), the Basic and Applied Basic Research Foundation of Guangdong Province (2021B1515130002), and Soft Science Research Project of Guangdong Province (2017B030301013). This work also gratefully acknowledges support from the U. S. Department of Energy (DOE), Office of Energy Efficiency and Renewable Energy, Vehicle Technologies Office.

Conflicts of interest

The authors declare no competing interests.

Notes and references

1. M. Cai, Y. Dong, M. Xie, W. Dong, C. Dong, P. Dai, H. Zhang, X. Wang, X. Sun, S. Zhang, M. Yoon, H. Xu, Y. Ge, J. Li and F. Huang, *Nat. Energy*, 2023, **8**, 159-168.
2. Y. Zhang, Y. Katayama, R. Tatara, L. Giordano, Y. Yu, D. Fraggedakis, J. G. Sun, F. Maglia, R. Jung, M. Z. Bazant and Y. Shao-Horn, *Energy Environ. Sci.*, 2020, **13**, 183-199.
3. C. Lin, J. Li, Z. W. Yin, W. Huang, Q. Zhao, Q. Weng, Q. Liu, J. Sun, G. Chen and F. Pan, *Adv. Mater.*, 2023, **36**, 2307404.
4. J. Zhang, P. F. Wang, P. Bai, H. Wan, S. Liu, S. Hou, X. Pu, J. Xia, W. Zhang, Z. Wang, B. Nan, X. Zhang, J. Xu and C. Wang, *Adv. Mater.*, 2022, **34**, 2108353.
5. X. Wang, H. Ren, Y. Du, Z. Li, W. Zhao, H. Ji, H. Yi, Q. Pan, J. Liu, Z. Lou, L. Zhou, F. Pan and Q. Zhao, *Nano Energy*, 2024, **125**, 109537.
6. H. Ren, W. Zhao, H. Yi, Z. Chen, H. Ji, Q. Jun, W. Ding, Z. Li, M. Shang, J. Fang, K. Li, M. Zhang, S. Li, Q. Zhao and F. Pan, *Adv. Funct. Mater.*, 2023, **33**, 2302622.
7. A. Yano, M. Shikano, A. Ueda, H. Sakaebe and Z. Ogumi, *J. Electrochem. Soc.*, 2016, **164**, A6116-A6122.
8. W. Ding, H. Ren, Z. Li, M. Shang, Y. Song, W. Zhao, L. Chang, T. Pang, S. Xu, H. Yi, L. Zhou, H. Lin, Q. Zhao and F. Pan, *Adv. Energy Mater.*, 2024, **14**, 2303926.
9. K. Kim, D. Hwang, S. Kim, S. O. Park, H. Cha, Y. S. Lee, J. Cho, S. K. Kwak and N. S. Choi, *Adv. Energy Mater.*, 2020, **10**, 2000012.
10. B. L. D. Rinkel, D. S. Hall, I. Temprano and C. P. Grey, *JACS*, 2020, **142**, 15058-15074.
11. Y. Yan, S. Weng, A. Fu, H. Zhang, J. Chen, Q. Zheng, B. Zhang, S. Zhou, H. Yan, C.-W. Wang, Y. Tang, H. Luo, B.-W. Mao, J. Zheng, X. Wang, Y. Qiao, Y. Yang and S.-G. Sun, *ACS Energy Lett.*, 2022, **7**, 2677-2684.
12. C. L. Campion, W. T. Li and B. L. Lucht, *J. Electrochem. Soc.*, 2005, **152**, A2327-A2334.
13. G. G. Amatucci, J. M. Tarascon and L. C. Klein, *Solid State Ionics*, 1996, **83**, 167-173.
14. M. He, C.-C. Su, C. Peebles and Z. Zhang, *J. Electrochem. Soc.*, 2021, **168**, 010505.
15. C.-C. Su, M. He, M. Cai, J. Shi, R. Amine, N. D. Rago, J. Guo, T. Rojas, A. T. Ngo and K. Amine, *Nano Energy*, 2022, **92**, 106720.
16. E. Markevich, G. Salitra and D. Aurbach, *ACS Energy Lett.*, 2017, **2**, 1337-1345.
17. T. Fan, W. Kai, V. K. Harika, C. Liu, A. Nimkar, N. Leifer, S. Maiti, J. Grinblat, M. N. Tsubery, X. Liu, M. Wang, L. Xu, Y. Lu, Y. Min, N. Shpigel and D. Aurbach, *Adv. Funct. Mater.*, 2022, **32**, 2204972.
18. Z. Wang, Z. Sun, Y. Shi, F. Qi, X. Gao, H. Yang, H. M. Cheng and F. Li, *Adv. Energy Mater.*, 2021, **11**, 2100935.
19. A. Zhang, Z. Bi, G. Wang, S. Liao, P. Das, H. Lin, M. Li, Y. Yu, X. Feng, X. Bao and Z.-S. Wu, *Energy Environ. Sci.*, 2024.
20. D. Aurbach, E. Markevich and G. Salitra, *JACS*, 2021, **143**, 21161-21176.
21. N. Xu, J. Shi, G. Liu, X. Yang, J. Zheng, Z. Zhang and Y. Yang, *J. Power Sources Adv.*, 2021, **7**, 100043.
22. C.-C. Su, M. He, R. Amine, Z. Chen, R. Sahore, N. Dietz Rago and K. Amine, *Energy Storage Mater.*, 2019, **17**, 284-292.
23. Y. Yang, J. Wang, Z. Li, Z. Yang, B. Wang and H. Zhao, *ACS Nano*, 2024, **18**, 7666-7676.
24. J. Hu, W. Ren, X. Chen, Y. Li, W. Huang, K. Yang, L. Yang, Y. Lin, J. Zheng and F. Pan, *Nano Energy*, 2020, **74**, 104864.
25. C. Yan, H.-R. Li, X. Chen, X.-Q. Zhang, X.-B. Cheng, R. Xu, J.-Q. Huang and Q. Zhang, *JACS*, 2019, **141**, 9422-9429.
26. X. Bogle, R. Vazquez, S. Greenbaum, A. v. W. Cresce and K. Xu, *J. Phys. Chem. Lett.*, 2013, **4**, 1664-1668.

27. Z. Yu, H. Wang, X. Kong, W. Huang, Y. Tsao, D. G. Mackanic, K. Wang, X. Wang, W. Huang, S. Choudhury, Y. Zheng, C. V. Amanchukwu, S. T. Hung, Y. Ma, E. G. Lomeli, J. Qin, Y. Cui and Z. Bao, *Nat. Energy*, 2020, **5**, 526-533.
28. R. Xu, C. Yan, Y. Xiao, M. Zhao, H. Yuan and J.-Q. Huang, *Energy Storage Mater.*, 2020, **28**, 401-406.
29. J. Zheng, J. Lu, K. Amine and F. Pan, *Nano Energy*, 2017, **33**, 497-507.
30. H. Zhang, Y. Huang, Y. Wang, L. Wang, Z. Song, H. Wang, C. Xu, X. Tian, S. Wang, J. Fang, W. Zhao, H. Cao, X. Yao, J. Yang, R. Tan, L. Yang, F. Pan and Y. Zhao, *Energy Storage Mater.*, 2023, **62**, 102951.
31. W. Dong, B. Ye, M. Cai, Y. Bai, M. Xie, X. Sun, Z. Lv and F. Huang, *ACS Energy Lett.*, 2023, **8**, 881-888.
32. W. Kong, J. Zhang, D. Wong, W. Yang, J. Yang, c. schulze and X. Liu, *Angew. Chem. Int. Ed.*, 2021, **60**, 27102-27112.
33. S. Chen, G. Zheng, X. Yao, J. Xiao, W. Zhao, K. Li, J. Fang, Z. Jiang, Y. Huang, Y. Ji, K. Yang, Z.-W. Yin, M. Zhang, F. Pan and L. Yang, *ACS Nano*, 2024, **18**, 6600-6611.
34. M. Malik, K. H. Chan and G. Azimi, *Rsc Adv.*, 2021, **11**, 28014-28028.
35. Z. Wu, G. Zeng, J. Yin, C.-L. Chiang, Q. Zhang, B. Zhang, J. Chen, Y. Yan, Y. Tang, H. Zhang, S. Zhou, Q. Wang, X. Kuai, Y.-G. Lin, L. Gu, Y. Qiao and S.-G. Sun, *ACS Energy Lett.*, 2023, **8**, 4806-4817.
36. C. Yogi, D. Takamatsu, K. Yamanaka, H. Arai, Y. Uchimoto, K. Kojima, I. Watanabe, T. Ohta and Z. Ogumi, *J. Power Sources*, 2014, **248**, 994-999.
37. J. Kikkawa, S. Terada, A. Gunji, T. Nagai, K. Kurashima and K. Kimoto, *J. Phys. Chem. C*, 2015, **119**, 15823-15830.
38. A. Yano, N. Taguchi, H. Kanzaki, M. Shikano and H. Sakaebe, *J. Electrochem. Soc.*, 2021, **168**, 050517-050517.
39. A. Nimkar, N. Shpigel, F. Malchik, S. Bublil, T. Fan, T. R. Penki, M. N. Tsubery and D. Aurbach, *ACS Appl. Mater. Interfaces*, 2021, **13**, 46478-46487.
40. W. Zhang, S. Zhang, L. Fan, L. Gao, X. Kong, S. Li, J. Li, X. Hong and Y. Lu, *ACS Energy Lett.*, 2019, **4**, 644-650.
41. L. Gireaud, S. Grugeon, S. Laruelle, S. Pilard and J. M. Tarascon, *J. Electrochem. Soc.*, 2005, **152**, A850-A857.
42. Y.-C. Lu, A. N. Mansour, N. Yabuuchi and Y. Shao-Horn, *Chem. Mater.*, 2009, **21**, 4408-4424.
43. S. Tan, Z. Shadike, J. Li, X. Wang, Y. Yang, R. Lin, A. Cresce, J. Hu, A. Hunt, I. Waluyo, L. Ma, F. Monaco, P. Cloetens, J. Xiao, Y. Liu, X.-Q. Yang, K. Xu and E. Hu, *Nat. Energy*, 2022, **7**, 484-494.
44. Y. Zhang, D. Krishnamurthy and V. Viswanathan, *J. Electrochem. Soc.*, 2020, **167**, 070554.
45. B. Ravdel, K. M. Abraham, R. Gitzendanner, J. DiCarlo, B. Lucht and C. Campion, *J. Power Sources*, 2003, **119-121**, 805-810.
46. C. L. Campion, W. T. Li, W. B. Euler, B. L. Lucht, B. Ravdel, J. F. DiCarlo, R. Gitzendanner and K. M. Abraham, *Electrochem. Solid State Lett.*, 2004, **7**, A194-A197.
47. K. Kim, I. Park, S.-Y. Ha, Y. Kim, M.-H. Woo, M.-H. Jeong, W. C. Shin, M. Ue, S. Y. Hong and N.-S. Choi, *Electrochim. Acta*, 2017, **225**, 358-368.
48. J. Liu, P. Bian, J. Li, W. Ji, H. Hao, A. Yu, *J. Power Sources*, 2015, **286**, 380-387.
49. C. Han, Y.-B. He, M. Liu, B. Li, Q.-H. Yang, C.-P. Wong, F. Kang, *J. Mater. Chem. A*, 2017, **5**, 6368-6381.
50. A. Van der Ven, M. K. Aydinol and G. Ceder, *J. Electrochem. Soc.*, 1998, **145**, 2149-2155.
51. M. Hirooka, T. Sekiya, Y. Omomo, M. Yamada, H. Katayama, T. Okumura, Y. Yamada and K. Ariyoshi, *J. Power Sources*, 2020, **463**, 228127.
52. J.-H. Shim, K.-S. Lee, A. Missyul, J. Lee, B. Linn, E. C. Lee and S. Lee, *Chem. Mater.*, 2015, **27**, 3273-3279.
53. B. Zhang, L. Wang, Y. Zhang, X. Wang, Y. Qiao and S.-G. Sun, *J. Chem. Phys.*, 2023, **158**, 054202.
54. Y. Lu, C.-Z. Zhao, J.-Q. Huang and Q. Zhang, *Joule*, 2022, **6**, 1172-1198.
55. T. H. Wan, M. Saccoccio, C. Chen and F. Ciucci, *Electrochim. Acta*, 2015, **184**, 483-499.
56. A. Rensmo, E. K. Savvidou, I. T. Cousins, X. Hu, S. Schellenberger and J. P. Benskin, *Environ. Sci-Proc. Imp.*, 2023, **25**, 1015-1030.
57. Wang, Z. Li, Y. Hou, Z. Hao, Q. Zhang, Y. Ni, Y. Lu, Z. Yan, K. Zhang, Q. Zhao, F. Li and J. Chen, *Chem. Soc. Rev.*, 2023, **52**, 2713-2763.

58. G. Ma, L. Wang, J. Zhang, H. Chen, X. He, Y. Ding, *Prog. Chem.*, 2016, 28, 1299-1312.
59. E. Fan, L. Li, Z. Wang, J. Lin, Y. Huang, Y. Yao, R. Chen, F. Wu, *Chem. Rev.*, 2020, **120**, 7020-7063.
60. F. Arshad, L. Li, K. Amin, E. Fan, N. Manurkar, A. Ahmad, J. Yang, F. Wu, R. Chen, *ACS Sustainable Chem. Eng.*, 2020, **8**, 13527-13554.